Available online at www.sciencedirect.com

SciVerse ScienceDirect

Journal of the European Ceramic Society 32 (2012) 1105–1116

www.elsevier.com/locate/jeurceramsoc

Synthesis, characterization, and wear and friction properties of variably structured SiC/Si elements made from wood by molten Si impregnation

Rajnish Dhiman [a], Kuldeep Rana [b], Erman Bengu [b], Per Morgen [a,*]

[a] *Department of Physics and Chemistry, University of Southern Denmark, Campusvej 55, 5230, Denmark*
[b] *Department of Chemistry, Bilkent University, Bilkent, 06800 Ankara, Turkey*

Received 28 July 2011; received in revised form 15 November 2011; accepted 21 November 2011
Available online 16 December 2011

Abstract

We have synthesized pre-shaped SiC/Si ceramic material elements from charcoal (obtained from wood) by impregnation with molten silicon, which takes place in a two-stage process. In the first process, a porous structure of connected micro-crystals of β-SiC is formed, while, in the second process, molten Si totally or partly infiltrates the remaining open regions. This process forms a dense material with cubic (β-)SiC crystallites, of which the majority is imbedded in amorphous Si. The synthesis of preshaped "sprocket" elements demonstrates that desired shapes of such a dense SiC/Si composite ceramic material can be achieved, thus suggesting new industrial applications.

The structure and composition of numerous as-synthesized samples were characterized in detail by using a wide range of techniques. Wear and friction properties were also investigated, with polished samples. The properties found for the present samples are very promising for abrasive applications and for new generation brake systems.

Keywords: SiC; Precursors-organic; Composites; Electron microscopy; Structural applications

1. Introduction

Silicon carbide is among the most sought ceramic and semiconducting materials for industrial applications because of its low mass density, high-thermal conductivity (350–490 $W\,m^{-1}\,K^{-1}$),[1] strong resistance towards oxidation, and high mechanical strength. Silicon carbide is also a wide band gap (2.39–3.33 eV)[2] semiconducting material with high electron mobility, high breakdown electric field strength (3–5 MV/cm), in its crystalline forms,[1] as well as a high oxidation resistance, and etch-resistant properties, making it eminently suitable for electronic and optical applications at high temperatures, high frequencies, and high powers.[3] Such qualities make it applicable with different functions in integrated biomaterials and in light-weight/high-strength structures.[4]

During the last two decades, biological materials[5–8] have been favoured as raw materials for synthesizing engineering ceramics and composites. Natural materials like rice hulls,[9] cotton fibers[10] and woods from different kind of trees[11–20] have thus been used as the starting material. The advantage of using wood as starting material is its tendency to retain the original shape. Thus SiC components have been successfully synthesized from wood using methods such as molten silicon impregnation,[10–16] silicon vapour impregnation,[17] carbothermal reduction after tetraethyl orthosilicate (TEOS) impregnation,[6,18] and shape memory synthesis using SiO vapour impregnation.[19,20] In the molten silicon impregnation method, molten silicon is forced to penetrate into the pore channel system of previously carburized wood by capillary forces and spontaneous wetting, undergoing a local solid–liquid reaction to form β-SiC. This method nearly retains the shape of the starting wood as a crystallized structure, in addition to the filling or capping of pores and voids with silicon. Thus, the sample produced in this way is actually a more-or-less dense, composite structure of silicon and SiC. It is very important to understand the synthesis mechanism of these SiC/Si ceramics. Despite a lot of work already reported on molten silicon impregnation of carbon obtained from wood, there are only a few attempts[13,21] reported studying the details of the formation mechanism of SiC in the ceramic but no conclusions are given for the entire composite system (SiC/Si) and the role of the silicon for the properties of the resulting material. It is also of interest to study the wear and friction properties of preformed

* Corresponding author. Tel.: +45 6550 3529; fax: +45 6615 8780.
E-mail address: per@ifk.sdu.dk (P. Morgen).

0955-2219/$ – see front matter © 2011 Elsevier Ltd. All rights reserved.
doi:10.1016/j.jeurceramsoc.2011.11.029

SiC/Si structures to test their applicability for friction and abrasion purposes, as these would not require post-synthesis forming or shaping processes. There are numerous studies on wear and friction properties of conventionally made SiC ceramics.[22–29] However, very few reports have focused on the wear properties of SiC/Si composites synthesized from natural products.[30]

In this work, the silicon impregnation method has been used to fabricate "sprocket shaped" SiC/Si structures from wood. Thus it is realized, how this low cost synthesis of variably structured SiC/Si samples with predefined shapes could make them usable in any shapes, as in highly abrasive elements for the automotive industry, i.e. in advanced brake systems. Similarly, they could be seen as alternatives to alumina when used for high temperature applications, where especially their high thermal conductivity could be explored. This synthesis route could also be seen as an important method for making structural (predefined shapes) parts of SiC composite materials for nuclear fusion reactors and in heat engines.[31–33] We have carefully explored the reaction mechanisms and can now confirm that the synthesis of SiC/Si ceramic is a two-stage process (from a pure carbon preform), where we can point out the important role of silicon for the ceramic material formation, and for its final properties. We have analysed many products formed from wooden preforms by Si-impregnation, using X-ray diffraction (XRD) for crystal structure determination, scanning electron microscopy (SEM) for imaging the surface morphology, X-ray photo electron spectroscopy (XPS) for determining the physical and chemical surface compositions, Auger electron spectroscopy with depth profiling for determination of in depth physical and chemical compositions, nano indentation for evaluation of hardness properties, and specific surface area measurements. A series of experiments have finally been made to study tribological properties like friction and wear of polished surfaces of these samples.

2. Experimental

Wooden samples were carved into three different shapes, cylindrical discs, sprocket shapes, and rectangular blocks of different sizes roughly ranging from 10 mm to 15 mm in length, 7 mm to 10 mm in breadth and 5 mm to 8 mm in height. Samples were made with different kind of woods such as Indian pine (*Pinus* sp.), Indian mango (*Mangifera indica*), Silk cotton tree (*Bombax ceiba*), Indian blackberry (*Syzygium cumini*), Cutch tree (*Acacia catechu*), Danish beech (*Fagus sylvatica*), etc. Most of the results reported here are obtained with Danish beech wood. Sample names show the type of wood used to synthesize the sample. The sprocket shaped samples were carefully cut exactly perpendicular to an axial direction in the wood in order to achieve discs of uniform thickness after pyrolysis. Different geometries have been used to demonstrate that the end product ceramic can be obtained in desired shapes, thus proving the usefulness of the present synthesis route. Since length contraction during pyrolysis of wood is orientation dependent, the contractions along radial-, axial-, and tangential directions are different.[13,20,34–36] Pyrolysis of wood is done in three stages. During the first stage, samples were heated to 70 °C for 2 h to remove the moisture. Samples were then heated to 500 °C at a slow heating rate of 1 °C/min in the second stage. This stage involves the decomposition of the polyaromatic hydrocarbon polymers like cellulose, hemicellulose and lignin, to form a pure carbon structure.[13,20,36] The third stage is a crystallization process where samples are heated to 1200 °C at a higher heating rate of 5 °C/min for 6 h. This heating leads to crystallization and purification of the carbon structures. Chances of oxidation and burning of the wood were minimized by carrying out all the process steps in an argon flow. The pyrolysis of the woods resulted in the formation of porous carbon structures (carbon preforms) with a network of capillaries as shown in SEM images. Several carbon preforms were placed in an alumina crucible together with silicon powder and heated up to a temperature of 1500 °C ± 25 °C (to melt Si in contact with the carbon shapes), inside an alumina tube in a tubular furnace for 12 h.

The finished samples were characterized by X-ray diffraction (XRD) to check the Si:C stoichiometry and their crystal structures by using a Siemens Diffractometer D5000 and the XRD results were analysed with the X'pert High Score Plus™ software. The topographical microstructure was imaged with a SEM (Zeiss LEO 435 VP), and the composition was checked by the energy dispersive X-ray (EDX) technique with a RÖNTEC detector attached to the same SEM. The confirmation of the SiC structure was also done with a Raman microscope from Dilor, using the 514 nm Ar-ion laser line. For analyses of the surface compositions, AES was used with a 1 μm spot electron beam excitation in a Perkin Elmer 560 system (with about 1 nm depth of information) and XPS in a SPECS PHOIBOS 100 system® (with a 2 mm diameter area of study, and about 7 nm depth of information). Hardness measurements of the samples were carried out by nano indentation using a triboIndenter system from Hysitron. The specific surface area of the samples was obtained with a surface area analyser from Quantachrome. Rectangular blocks are used for all the above-mentioned characterizations. Further, dry wear testing of synthesized SiC/Si samples of cylindrical shapes has been conducted by using a high temperature ball-on-disc tribometer (CSM-THT). The samples used for this were first ground with SiC papers of different grit size and finally polished using diamond slurry on felt. During the ball-on-disc wear testing, samples were tested by sliding against commercial alumina balls of 6 mm diameter. These tests were conducted for a total travelled distance of 50 m under normal atmospheric conditions at room temperature with a relative humidity of 55% using loads of 1, 2, 4 and 5 Newtons (N).

3. Results and discussion

3.1. Confirmation of the nature of the SiC/Si composite

3.1.1. X-ray diffraction analysis

The XRD patterns confirm the formation of cubic (β-SiC) with some additionally un-reacted silicon as shown in Fig. 1. Table 1 lists the percentage of different phases present in the samples. The diffraction patterns of the samples show major peaks at $2\theta = 28.4°$, 35.5°, 41.3°, 47.2°, 59.8°, and 71.6°, which

Table 1
Percentage concentration of different polymorphs of SiC. Sample name shows the type of wood used to synthesize the sample.

Sample	Cubic/%	Si/%	SiO_2/%
Beech wood (1)	87.6	12	0.4
Beech-wood (1)-oxidized	94.7	4.5	0.8
Beech wood (2)	89.4	10.6	
Beech wood (3)	96.8	3.2	
Cutch tree	94.5	5.5	

corresponds to diffraction from the Si (1 1 1), SiC (1 1 1), SiC (2 0 0), Si (2 2 0), SiC (2 2 0) and SiC (3 1 1) planes.

The average grain size of the samples is found to be 93 nm and has been calculated by using a Williamson–Hall plot.[37] The Rietveld refinement[38,37] technique was used to obtain accurate values of lattice parameters of crystals and phases present in the crystal samples. The oxidation of sample Beech wood (1) for 3 h at 700 °C in air leads to decrease in percentage of un-reacted silicon from 12% to 4.5% (see Fig. 1 and Table 1). Thus the previously un-reacted silicon has now formed amorphous SiO_2, shown as a decrease in intensity of the Si peak at 28.3°, while the SiC peaks increase in intensity.

Table 1 summarizes the percentage distribution of cubic SiC, un-reacted Si and SiO_2 in some of the synthesized samples. The comparison of XRD results with experimental mass measurements is done in a subsection discussing the ceramic formation. The XRD patterns suggest that the samples made by silicon impregnation are more crystalline than for shape memory synthesis.[20]

3.1.2. SEM images

The SEM images of the SiC/Si samples and the starting carbon preforms are shown in Fig. 2. Fig. 2(a) shows the top surface of a carbon preform, which was cut perpendicular to an axial direction in the starting Danish beech wood. This image indicates two different kinds of pores or capillaries in the starting carbon structure originating from vessels and tracheid channels,

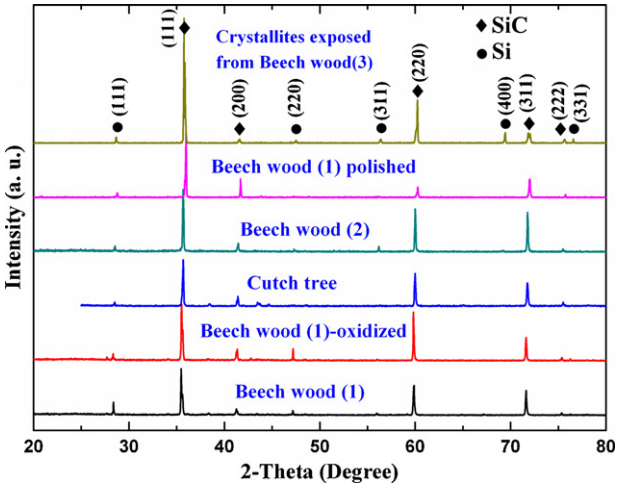

Fig. 1. XRD patterns of the samples synthesized from beech wood, and cutch tree. XRD pattern from individual crystallites is also shown (explained later). Sample name shows the type of wood used to synthesize the sample.

the bigger pores having a size of 20–25 μm while the smaller pores have sizes in the range of 5–8 μm. Fig. 2(b) shows the internal capillary system of the carbon preform when it is cleaved along the axial direction. Fig. 2(c) and (d) are images of the top surface of the samples after conversion to the SiC/Si ceramic at different magnifications, corresponding to the preforms in Fig. 2(a). SiC and silicon regions have also been marked in the images. The top surface of these samples appears as having the individual SiC crystals embedded inside silicon. Fig. 2(c) and (d) indicates significant redistribution during the solid phase reaction of carbon with silicon. All the pores have vanished near the top surface. Fig. 2(e) and (f) shows the images of the sample from inside. The bigger pores, which appear as channels in the starting carbon (Fig. 2(b)) are still preserved after the SiC/Si formation as shown (labelled as channels) in Fig. 2(e), but they are not uniform as before the onset of the process, as SiC crystals have expanded during growth to make it non uniform. The smaller pores of the starting carbon have totally vanished after the reaction due to SiC crystallite formation (Compare Fig. 2(a and b) with (c–f)). The starting carbon framework has been redistributed during the solid phase reaction and the SiC crystallites have nucleated everywhere, which is evident from the Figs. 2(c–f). Fig. 2(f) shows the individual SiC crystals formed inside the SiC/Si sample. Comparison of Fig. 2(a) and (b) with (c–f) proves that the capillaries pull the molten silicon inside in the solid phase contact reaction to form SiC/Si. The presence of Si and SiC crystallites in the composite is explained further in Section 3.2.

3.1.3. XPS analysis

XPS spectra of two samples made from Danish beech wood are shown in Fig. 3 and compared with a standard SiC reference sample (6H-SiC wafer). Electrons with kinetic energies from 200 eV to 1260 eV have been recorded, covering the range of binding energies from 1053 eV to −7 eV, as they are excited with an Mg X-ray source. In the figures the kinetic energies have been converted to binding energies (relevant only for the photoelectron peaks). The sampled area has a diameter of 2 mm. All the spectra show the presence of carbon, oxygen and silicon. The reference sample (a 6H-SiC wafer) also shows Ar (2p) and N (1s) photoelectron peaks. This sample had been sputtered with argon for a short time to remove the contamination on the top surface, before the XPS measurements. Small amounts of calcium (≈0.5% concentration) are seen in the two samples, coming from the starting wood.[39]

The processed samples are oxidized due to the handling in air after the synthesis. The silicon to carbon ratio in these two samples are equal, but different from the ratio of the reference sample, which is due to different amounts of oxide and adsorbed carbon species at the surfaces of the samples. The general shape of the wide scan XPS spectra varies with the density and structure of the samples. The inelastic lower-energy background below the sharp peaks depends on the sample density and morphology. The 6H-SiC sample has the flattest background below the O (1s) (720 eV) and O_{KLL} peaks (500 eV) (i.e. at lower kinetic energies), while the silicon-impregnated samples show a higher slope of the background in this region. Different background slopes below the oxygen signals (lower kinetic energies) indicate

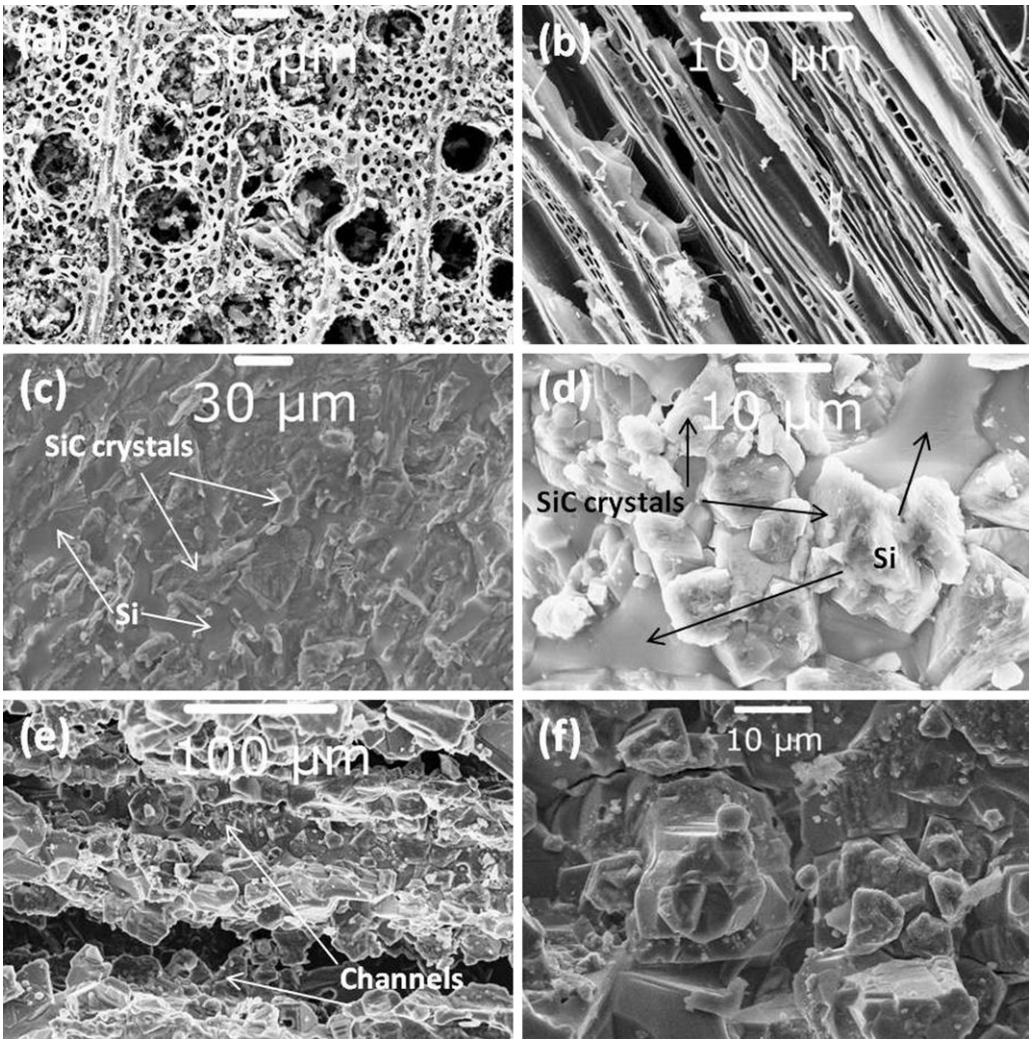

Fig. 2. SEM images of two carbon preforms (a) and (b) from Danish beech wood; and SiC/Si samples (c)–(f). (a) is perpendicular to axial direction; (b) is along the axial direction. (c) and (d) are the top surface of sample, SiC/Si replica of (a) at the different magnifications. (e) and (f) are images from inside the sample, (e) is the SiC/Si replica of (b). (f) shows SiC crystals imbedded in silicon.

differences in the in-depth distributions of oxygen in the samples[40] and effects of roughness. Higher slopes indicate deeper penetration of oxygen.

The reported concentrations of the impregnated samples seem to indicate, when compared to the (mildly sputtered) reference sample, that the amount of carbon in the top layers of the impregnated samples is slightly higher than for this reference sample. We believe that most of this excess carbon (compared to Si) comes from the ambient during handling of the samples, and a variable degree of oxidation, which tends to lower the Si concentration at the surface. We thus do not detect any excess of Si over SiC with this technique, even averaging over an area of 2 mm. It is therefore interesting to check, with a better resolution, and deeper in the samples, how their local compositions change. This is done with Auger electron spectroscopy (AES).

3.1.4. Auger analysis

In order to better access the local concentration of the samples beneath the oxidized surface, and contamination layers, we used electron beam excited AES in combination with Ar^+-ion sputtering.

Fig. 4 shows the result of such a sputter profile measurement. This analysis is done with AES excited with a focused electron beam (1 μm) of 5 keV energy, focused on a SiC crystal-like hump on the surface, and the surface is repeatedly bombarded for periods of 10 minutes with Ar-ions to remove the upper layers, and then analysed. Each 10 min sputtering interval would remove 10 Å of a uniform, flat sample as calculated by the SRIM code[41,42] for the present experimental conditions. Fig. 4(a) shows peaks at 92 eV (Si_{L23VV}), 272 eV (C_{KLL}), 290 eV (Ca_{LMM}), and 505 eV (O_{KLL}). From the sputter profile it can clearly be seen that the intensity of the oxygen peak is reduced with the sputtering time while the intensity of the carbon and silicon peaks are increasing. From the spectra we can also see the presence of calcium, which is an essential nutritional component of beech wood.[39] Fig. 4(b) shows the corresponding atomic percentage of Si, C and O with depth. From the measured values, as shown systematically in Fig. 4(b), we judge the deviation of the concentrations from smooth curves to be less than 2.5%, which

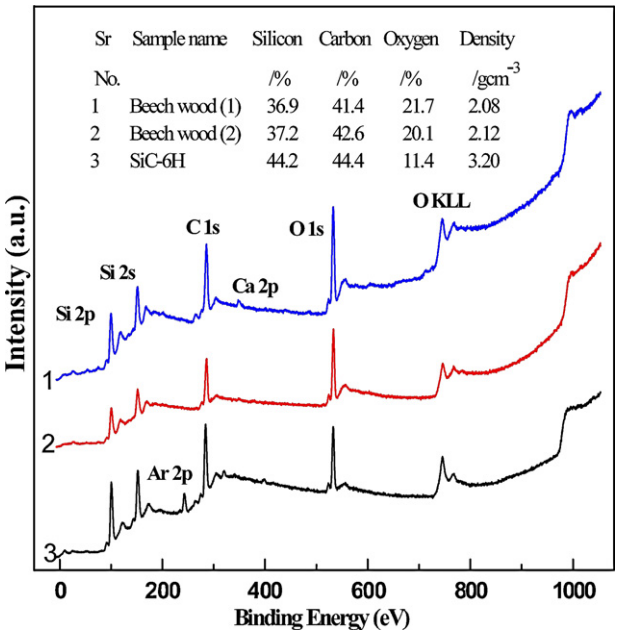

Fig. 3. XPS spectra of two samples quoted as 1 & 2 (both synthesized from Danish beech wood) in the figure, and the 6H-SiC reference sample quoted as 3. The inset table in the figure shows the percentage concentrations of these samples as derived by the Casa XPS™ software.

we state as the experimental accuracy of the method as applied to this sample. We can clearly see the gradual approach to a nearly 1:1 stoichiometry of silicon and carbon in depths well below the oxidized surface, but with some local fluctuations, which are probably due to the non-uniform character of the sample.

3.1.5. Raman analysis

Raman spectroscopy can be used to distinguish the individual polymorphic types of SiC[43,44] and it also confirms the formation of β-SiC in the samples. The β-SiC has a zinc blende like structure with the smallest unit cell of all the SiC polymorphs. Bulk β-SiC has two optical modes at the Γ point of the Brillouin zone, a transverse optic (TO) mode at 796 cm^{-1} and a longitudinal optic (LO) mode at 972 cm^{-1}.[44]

The XRD results showed around 90% β-SiC as a major phase and the rest as un-reacted silicon. The Raman spectra are also showing peaks of β-SiC and silicon, which thus confirms the presence of SiC and silicon in the samples. Since the Raman lines of SiC samples are rather broad, the resolution of Raman microscope was set to ±4 cm^{-1}. From the positions of the phonon peaks shown in Fig. 5 and summarized in Table 2, it can clearly be concluded that all peaks are falling in the vicinity of 796 cm^{-1} and 972 cm^{-1}, which are known as TO and LO modes for β-SiC, respectively. The full width at half maximum (FWHM) of these peaks is in the range of 22–26 cm^{-1}, which suggests that the samples are having stacking faults.

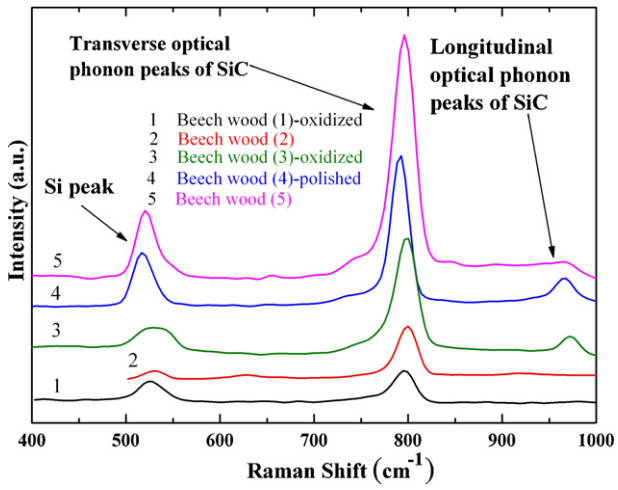

Fig. 5. Raman spectra of the samples (all synthesized from Danish beech wood).

Table 2
Peak positions in the Raman spectra of samples and suggestions for the polymorphs.

Sample	Peak positions/cm^{-1} (±4 cm^{-1})	Suggestions for polymorph/cm^{-1} [43,44]
Beech wood (1)-oxidized	795.6	3C (796 and 972)
Beech wood (2)	799.5	3C (796 and 972)
Beech wood (3)-oxidized	798.3, 971.5	3C (796 and 972)
Beech wood (4)-polished	791.3, 965.4	3C (796 and 972)
Beech wood (5)	796.1, 967.3	3C (796 and 972)

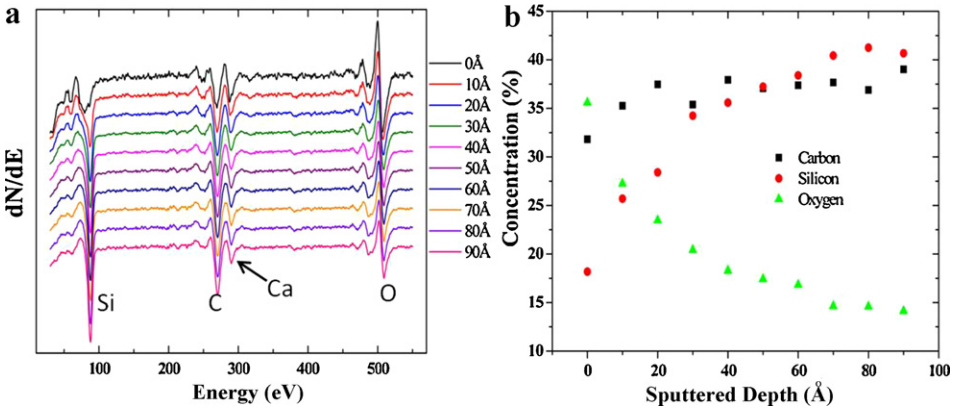

Fig. 4. (a) Sputter profile of a SiC crystallite hump on the surface of a sample made from Danish beech wood. (b) Relative percentage concentration of Si, C and O with the depth, from the Auger spectra.

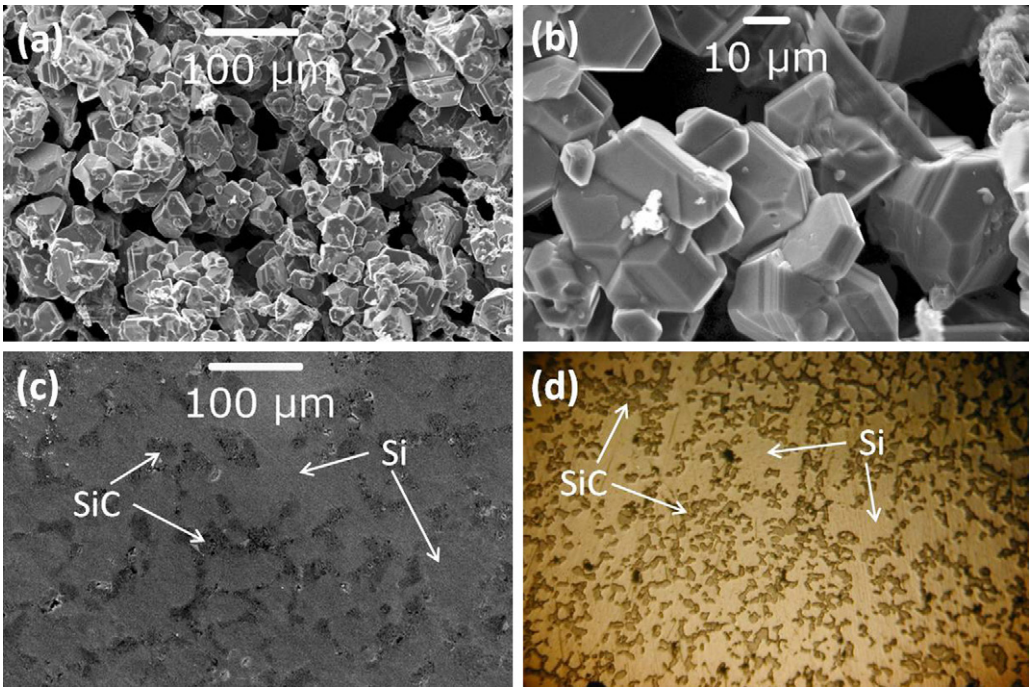

Fig. 6. SEM images of individual crystallites (a) and (b) at different magnifications (inside the sample which was broken on purpose and taken out after 6 h processing). (c) SEM and (d) optical microscope image of a polished sample surface. Sample made from Danish Beech wood.

3.2. Ceramic formation

In the present method, carbon preforms are impregnated with molten silicon and capillary action pulls the liquid silicon into the pores. All details of the pyrolysis process (see also above) to obtain the carbon preforms themselves and characterization by XRD, SEM and Raman, including TGA of wood have already been given.[20]

After being drawn into the carbon structures, Si reacts with carbon at a temperature of 1500 ± 25 °C, forming a compact, low surface area SiC/Si composite material. Silicon melts at 1410 °C and the liquid enters into the pores undergoing a solid–liquid reaction to form SiC as follows:

$$\mathrm{C\,(solid) + Si\,(liquid)} \overset{1500\,^{\circ}\mathrm{C}}{\longrightarrow} \mathrm{SiC\,(solid)}$$

3.2.1. Role of silicon

The synthesis of SiC/Si ceramics from carbon preforms involves a two-step process. In the first step molten silicon infiltrates the capillaries of the carbon element to react with the carbon to form crystalline SiC and, in our case this process runs for more than 5 h to process all the carbon. The second step involves further infiltration with molten Si until some kind of saturation. Molten silicon is readily available[13] in the capillaries in the beginning, but we have observed that its penetration becomes very slow at the end. The conversion of carbon to silicon was very well explained by Zollfrank et al.,[21] and some further details are given in the support material. The second – or last – step of ceramic formation, which involves further penetration into voids by the silicon melt, is very crucial and is responsible for keeping the whole ceramic together as a single solid unit. Almost all of the un-reacted silicon is amorphous in nature as observed from the XRD pattern of the polished sample, shown in Fig. 1.

We have carried out the silicon impregnation at 1500 °C under the argon flow and have checked the sample after the first stage. Fig. 6(a) and (b) shows the SEM images of the individual crystallites inside the sample having dimensions ranging from 15 to 40 μm. These images have been taken from inside the sample and this sample was taken out "prematurely" after 6 h. Thus only the first stage of reaction has been completed (in case of Fig. 6(a and b)), which has only resulted in the formation of SiC micro-crystals. Thus, Figs. 6(a) and (b) are snapshots of a sample after the first stage of the reaction. The XRD (Fig. 1) and Raman (Fig. 7c) of crystallites confirm that the samples after completion of this step are in the form of pure crystalline SiC. These individual crystallites can be removed from the exposed surface by gentle abrasion. Thus the pure SiC crystals formed after the first stage are not held strongly together, but the further addition of silicon (during the second stage) holds them strongly together, forming a dense unit.

If infiltration of Si into the voids (Fig. 6(a) and (b)) between the individual crystallites continues to fill them up completely, it would result in SiC/Si ceramics like the ones shown in Fig. 2(c)–(e), where they appear as very dense units. Fig. 6(c) and (d) shows the respective SEM and optical microscope images on the surface of a polished sample with this maximum density. The crystalline SiC inclusions appear as islands in the matrix of silicon. The SiC appears dark grey while silicon appears as light grey in the SEM image (Fig. 6(c)). Similarly, Si and SiC appear with different yellow brightness in optical microscope images (Fig. 6(d)). We have also produced a powder consisting of SiC micro-crystals from similar samples simply by etching away the

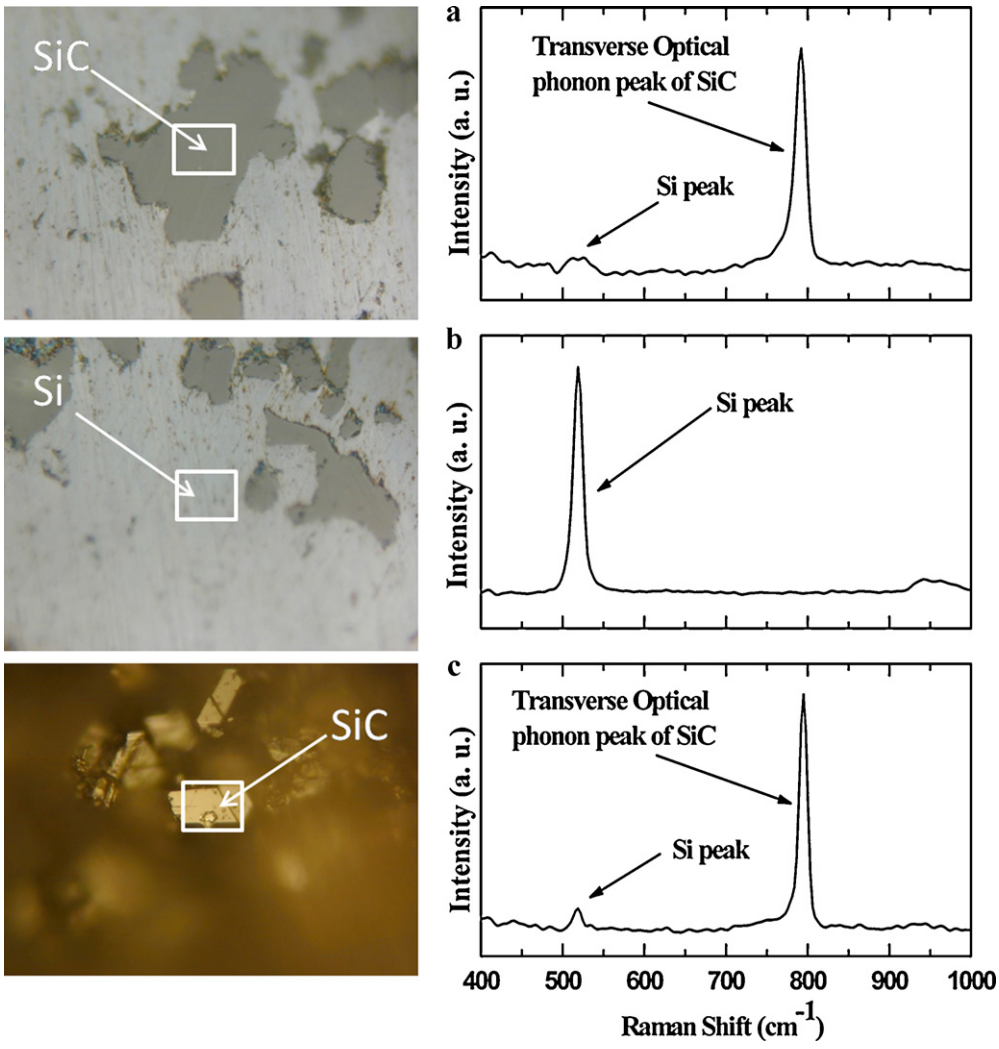

Fig. 7. Optical microscope images and their corresponding Raman spectrum (from the marked places) of a polished sample in (a) and (b), and SiC crystallite in (c). (a) a SiC region, (b) a Si region, and (c) a SiC crystallite. Sample made from Danish beech wood.

amorphous Si with a mixture of HF and HNO_3. It proves that this method can also be used to produce SiC micro-crystals, and it indirectly proves the role of amorphous silicon as the binder in these samples.

Fig. 7(a) and (b) shows the Raman spectra taken on a polished sample at the places marked in the optical microscope images on the left side in the figure. The optical microscope image in Fig. 7(a) shows a dark grey region and the corresponding Raman peak indicates β-SiC. Similarly, Fig. 7(b) shows the silicon region and the silicon peak in Raman. Fig. 7(c) shows the Raman spectrum over one of the SiC crystallites shown in the optical microscope image and as discussed previously in reference to Fig. 6(a) and (b). The results of Raman studies of the polished samples have also been confirmed by the EDX measurements as shown in Fig. 8. The EDX has been done at two different areas, at Si and SiC rich regions. The atomic percentages of respective areas are tabulated as the inserts in Fig. 8, which suggest the presence of Si and SiC phases in composite.

From the all the points in this discussion, it can now be concluded that silicon fills the voids between the individual crystallites and thereby helps in holding the SiC crystallites together to produce a dense piece of a solid material. Thus molten silicon plays the role of binder of individual crystallites. It prevents them from falling apart and creates a dense structure.

3.2.2. Determination of mass and density

In this analysis the carbon atoms are supposed to react with an equal number of Si atoms to form SiC. The density of the resultant product can therefore be calculated by using a simple formula:

$$D_{\text{composite}} = \left(D_{\text{carbon}} + D_{\text{carbon}} \times \frac{28.0855}{12} \right) \times \left(1 + \frac{M_{\text{Si}}}{M_{\text{SiC}}} \right), \quad (1)$$

where $D_{\text{composite}}$ is the calculated value of density of the sample, D_{carbon} is the density of the carbon preform of a particular sample, and M_{Si} and M_{SiC} are the masses of Si and SiC in the composite. The derivation of this formula and other equivalent formulae are given in supporting material.

The term $(D_{\text{carbon}} + D_{\text{carbon}} \times (28.0855/12))$ is the theoretical value of the density of SiC when only one additional atom of silicon is added to the carbon atoms of the

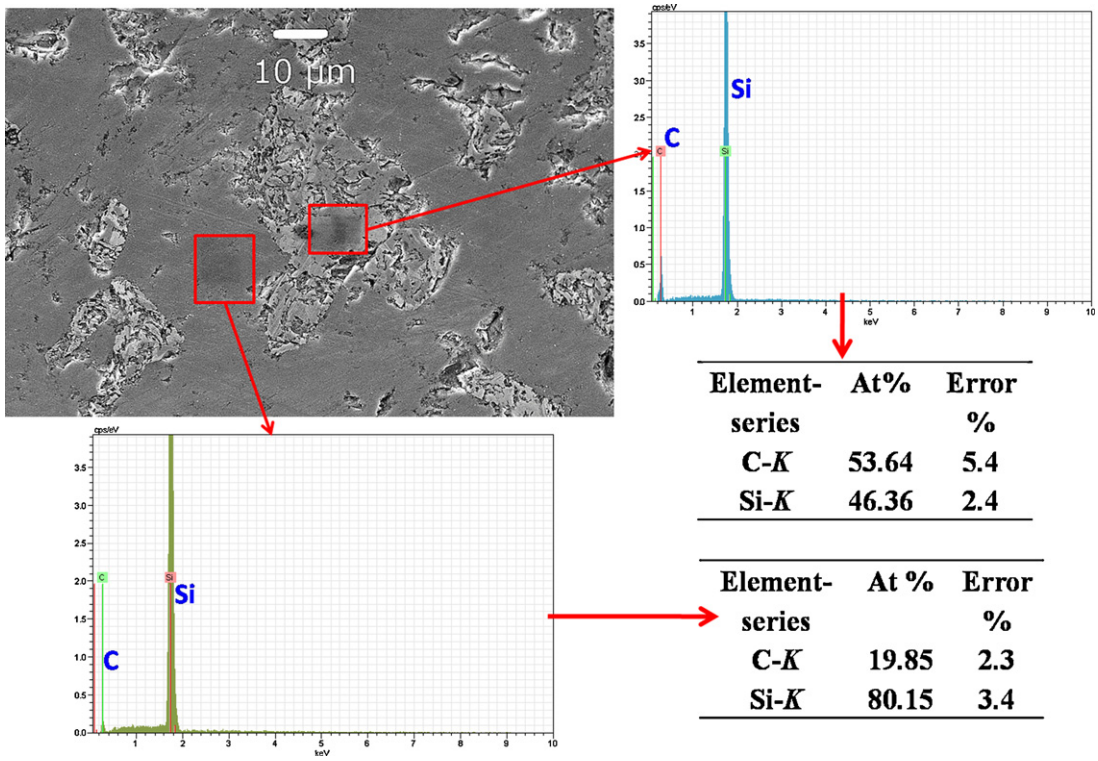

Fig. 8. SEM image and EDX at the marked places showing Si and SiC region in a polished sample. Sample made from Danish beech wood.

earlier framework. The additional term ($D_{carbon} + D_{carbon} \times (28.0855/12))(M_{Si}/M_{SiC})$ is due to the presence of un-reacted silicon inside the sample. The mass of the un-reacted silicon has been estimated by taking the difference of mass of final composite and the theoretical mass, which is given as ($M_{carbon} + M_{carbon} \times (28.0855/12)$).

The difference between experimental values and calculated values is between 0 and 8.1%. These deviations, although mostly small, may come from errors in the measurement of the volume of the sample and from the presence of other elements such as calcium in the original wood as seen from EDX, XPS, and Auger results. There is always a presence of oxygen, most likely adsorbed on the surface of the samples, but not accounted for in the model. In this model we have not considered any excess carbon because we have not found any signs of such unreacted carbon (less than 0.8%) in the TGA of SiC/Si, as shown in the supporting material.

The comparison of the percentage of silicon deduced from the change in mass of the samples (shown in Table 3), which is around 35–40%, and from XRD analysis (shown in Table 1), which is showing 5–12%, suggests that most of the silicon is present in its amorphous form.

From Table 3 it is concluded that all of the carbon preform material has been converted to crystalline SiC. Un-reacted Si fills and takes up the empty space in the samples and accounts for the additional 40% of the material (by mass). If and when there is good agreement between experimental and calculated values in the table, the use of Eq. (1) for the analysis seems justified, and the model presented here is then valid.

After the completion of the reaction process, most of the bigger pores in the starting wooden framework must have been filled with silicon or have been capped from the top, resulting in $\approx 0\ m^2\ g^{-1}$ specific surface areas (discussed later). There are still some voids or open channels inside the structural unit as shown in the SEM image in Fig. 2(d), which leads to a smaller value for the density of the SiC/Si composite (given in Table 3) than the density of bulk silicon ($2.32\ g\ cm^{-3}$) or bulk SiC ($3.2\ g\ cm^{-3}$). The present values are approximately similar to those obtained by Greil et al.[14] The starting carbon structure is with a honeycomb like structure of the bigger size pores, together with a distribution of small size pores as shown in Fig. 2(a). The smaller pores vanish quickly during the reaction of silicon with carbon to form SiC crystallites while the bigger pores (capillaries) may still remain in existence in the form of non uniform voids (see Fig. 2(d)), not having been completely filled by the molten silicon. Thus, overall it can be said that Si impregnation retains the starting bulk structure of the carbon preform while its microstructure (smaller pores) is lost during the formation of SiC crystallites. Fig. 9 shows, as an illustration of the procedures used here, how a compact, hard and lightweight sprocket shaped structure of SiC/Si can be formed from a preshaped wooden structure, when impregnated with molten silicon.

3.3. Hardness and specific surface area analyses

The hardness at various positions of one of the samples (synthesized from Danish beech wood) was measured by nano indentation with a Berkovich diamond indenter. The XRD, SEM, EDX and Raman measurements suggested different regions of SiC and Si on the samples, so local variations in hardness are expected, which was our reason for using nano indentation that also provides information about elastic modulus. The sample

Table 3
Calculated and experimental values of mass and density of the samples synthesized by silicon impregnation.

Sample name	Mass of carbon/g	Density of carbon/g cm^{-3}	Theoretical mass of SiC/g	Experimental mass of composite/g	Un-reacted silicon/%	Experimental value of density of composite/g cm^{-3}	Calculated value of density of composite/g cm^{-3}	Deviation from calculated value of density/%
Beech wood (1)	0.56	0.4	1.87	2.82	33.7	2	1.999	0.2
Beech wood (2)	0.25	0.37	0.83	1.37	39.4	2.08	2.079	≈0
Beech wood (3)	0.26	0.32	0.86	1.48	41.9	1.84	1.835	≈0
Beech wood (4)	0.25	0.37	0.83	1.14	27.5	1.78	1.696	4.8
Beech wood (5)	0.2	0.37	0.67	1.09	38.5	2.12	1.986	6.5
Beech wood (6)	0.29	0.34	0.96	1.59	39.8	2.06	1.904	8.1
Beech wood (7)	0.10	0.38	0.32	0.58	44.6	2.26	2.261	0.1
Beech wood (8)	0.07	0.36	0.24	0.46	47.3	2.31	2.299	0.5

used was flat, dense and polished with a finish down to 500 μm. The Oliver and Phaar method[45] is used to evaluate the hardness values using the loading and unloading curves, when load displacement curves are recorded under load-controlled mode. The load displacement curves show a hysteresis-like behaviour with elastic–plastic loading followed by an elastic unloading. The knowledge of the contact area between the indenter and the sample is very important. It is known that the plastic properties of the sample under observation can change the contact area and hence result in wrong values.[46] This happens mainly when a "pile up" or "sinking in" of the displaced material happens around the indentation spot. The ratio of h_c/h_{max}[45] indicates the tendency of the material to pile up, where h_{max} is the maximum depth of penetration during the indentation test and h_c is the final displacement after the complete unloading of the contact. If the ratio $h_c/h_{max} < 0.7$ then the contact area given by the Oliver–Phaar method is known to match very well with the true contact area, and if $h_c/h_{max} > 0.7$, then it may lead to large errors in contact area.[47] In this method the contact depth is estimated from the load displacement data using the following equation:

$$h_c = h_{max} - \varepsilon \frac{P_{max}}{S}, \tag{2}$$

where P_{max} is the maximum indentation load, S is the stiffness obtained from the unloading curve as $S = (dP/dh)_{P=P_{max}}$ and ε is a constant, which depends upon the indenter geometry; empirical studies have shown that $\varepsilon \approx 0.75$.

The hardness, H, and elastic modulus, E, are calculated using the following formulae:

$$H = \frac{P_{max}}{S}, \tag{3}$$

and

$$E = \frac{1}{\beta}\frac{\sqrt{\pi}}{2}\frac{S}{\sqrt{A}}, \tag{4}$$

where β is a constant, depending on the geometry of the indenter. Its value for the Berkovich indenter is 1.034. The area of the impression, A, is determined from the indenter shape function at the contact depth h_c and is properly calibrated.

The hardness values obtained for the samples vary between 10.7 and 31.4 GPa. From Table 4, giving the results, we can group our values in three sets. The first five values in this table have hardness values from 26.5 to 31.4 GPa (with a standard deviation (SD) of 2.30 GPa), and elasticity values ranging from 236.9 to 332.1 GPa (SD of 39.8 GPa), which matches the respective values for compact bulk SiC.[48] This set of values constitutes a first category. The following category has two values 10.7 and 12 GPa for hardness and elasticity values of 115.8 and 121.9 GPa, which, in turn, clearly match values for silicon.[49]

The third category has values varying from 17.1 to 22.3 GPa (SD of 2.32 GPa) for hardness and 169.9–261.9 GPa (SD of 35.5 GPa) for the elasticity values. This category most likely includes erroneous values due to an overestimation of area because of pile up during the indentation, since the h_c/h_{max} ratio

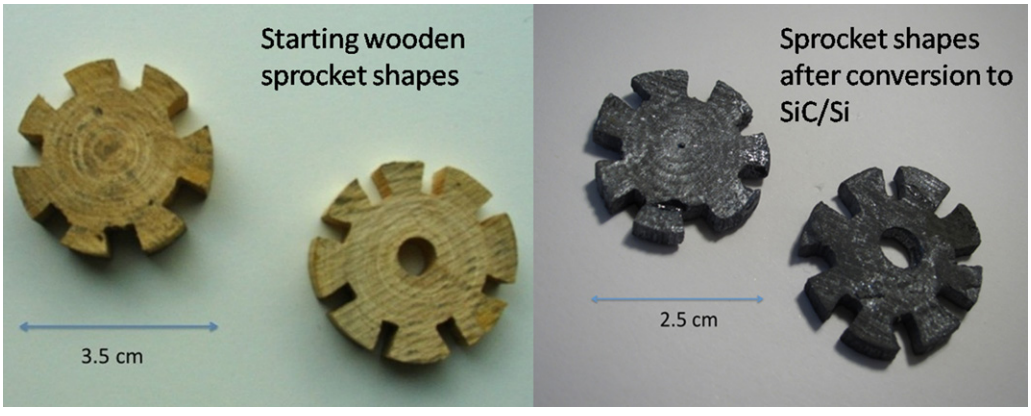

Fig. 9. Image of "sprocket shaped" Danish beech wood and converted SiC/Si structures.

Table 4
Hardness and Young's modulus values measured in different points on one sample, made from Danish beech wood.

S. no.	h_c/nm	Area/nm^2	Load/microN	$F = h_c/h_{max}$	Hardness/GPa	E/GPa
1	73.9	232736.3	7302.54	0.66	31.4	253.2
2	51.9	131368	3504.8	0.66	26.7	236.9
3	75.7	241581.1	6979.9	0.68	28.9	259.5
4	90	317848.4	8433.58	0.69	26.5	235.2
5	67.5	201649	6251.45	0.71	31	332.1
6	75.2	238709	2858.9	0.71	12	121.9
7	65.8	207725	2229.4	0.71	10.7	115.8
8	98.9	371146.5	6333.86	0.72	17.1	169.9
9	93.5	338434.7	6009.6	0.73	17.8	194.7
10	79.3	259817	4797.1	0.74	18.5	213.6
11	121.6	528854.5	8596.06	0.75	16.3	185
12	94.1	342117	7625.35	0.75	22.3	261.9

exceeds 0.7, as discussed above, or it may be due to the averaging of the contributions from both Si and SiC. Otherwise, these values may have been influenced by the non-uniform surface of the polished sample (see Fig. 2(f)) used for the indentation measurements.

The BET adsorption isotherm method is used to measure the specific surface areas of the samples. Initially, the samples are evacuated and degassed at 350 °C. After cooling them down to liquid nitrogen temperature, nitrogen gas at variable pressures is used to obtain six points on the BET adsorption isotherm, from which the specific surface area is calculated. The specific surface areas of the three samples have been measured and their respective values are found to be 0.33, 0.00 and 0.06 $m^2\,g^{-1}$. With these values, we can say that these samples are almost totally non-porous. This is understandable assuming that the molten silicon goes into the porous carbon framework and fills the holes up to a large extent, and caps the rest, and thus may not leave any passage for nitrogen to go inside and adsorb. The corresponding SEM pictures in the Figs. 2(c)–(f) show the presence of uniformly imbedded crystallites, indicating the absence of irregularities and defects, which could otherwise have acted as adsorption sites for the nitrogen gas.

3.4. Wear and friction properties

In this study, preformed SiC/Si structures (synthesized from Danish beech wood) with flat faces (as shown in Fig. 9) were used for experiments to test the wear and friction properties. The wear rate (W_r) was calculated by using the following equation:

$$W_r = \frac{W_v}{Fl}, \tag{5}$$

where W_v is the wear volume, F is the normal load (in N) applied on flat surface and l is the sliding distance.

Figs. 10(a) and (b) shows the SEM micrographs from the wear track of a tested SiC/Si composite under dry sliding conditions. The wear track shows a smooth, near-polished surface with some wear debris on the track. Experimental data of friction measurements (as shown in the support material) indicates an increase in the coefficient of friction (COF) in the beginning. It becomes constant afterwards, which may be attributed to removal of the initial surface roughness of the material. From the SEM images in Fig. 10(a) and (b), the main wear mechanism could be attributed to micro-cracking and pulling of the grains in the composite material, which results in cavity formation and, later, filling of these cavities by the wear debris.[25] Fig. 10(c) also shows the effect of normal load on COF (μ) at room temperature (25 °C). This figure indicates that there is no significant variation in the COF with normal loads up to 2 N. However, COF increases to an average value of 0.75 for loads of 4 and 5 N. These results are comparable with those of Dong et al.,[26] where α-SiC balls were used on SiC ceramics and μ was found to be 0.67 on average. Sang et al.,[29] have also reported similar values of COF for Si/SiC composite. Our values are slightly higher and it might be due to the rough surface and the presence of free SiC-crystallites, which get on top of the surface due to ploughing when the sample is polished. It is suggested that the SiC component in the SiC/Si composites leads to higher μ, accompanied by higher wear due to its abrasive nature, while the presence of Si in the composite matrix has a large impact on the morphology and adhesive friction, which actually also increases μ.[28] Silicon can thus react with oxygen in the alumina balls and cause formation of hard SiO_2 particles, which are excellent abrasives. Furthermore, Si by itself could stick to the alumina ball, causing an increase in the friction forces.

Fig. 10(d) shows the variation of the coefficient of friction with temperature at a constant normal load of 4 N. The figure shows a very small increase in the coefficient of friction with temperature. There is a step of 0.073 in μ from room temperature to 100 °C and after that there is slight increase of approximately 0.014 in μ with every 200 °C rise in temperature. This set of observations lies partly in region II and partly in region III of the transition diagram suggested by Dong et al.[26] The region II starts from room temperature to 250 °C approximately at normal loads less than 10 N and region III is constituted by COF values measured for the temperature range of 250–1000 °C at normal loads less than 10 N. This region is governed by tribo-oxidation reactions. Takadoum et al.,[27] have also studied the friction coefficient and properties of SiC/Si systems and found μ values varying in the range of 0.4–0.85 with increasing sliding distance at a relative humidity of 50%. The μ values found here are thus slightly higher than reported by others.[29,30]

The wear rate calculated by using Eq. (5) at normal load of 4 N in a sample of the SiC/Si composite is 6.6×10^{-4} mm^3/Nm

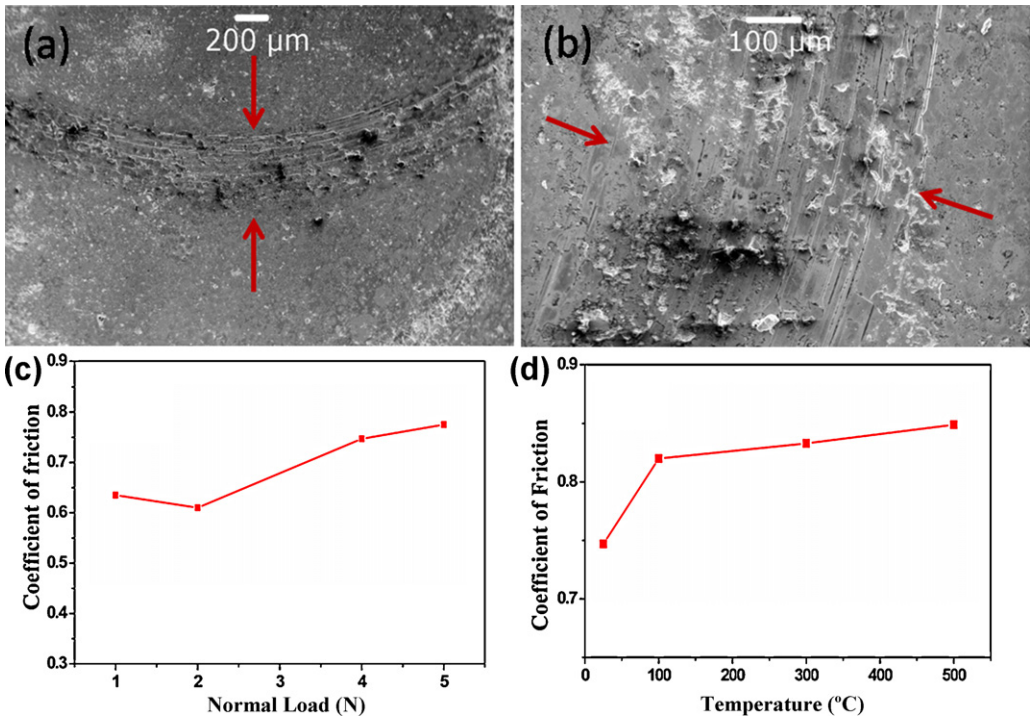

Fig. 10. (a) and (b) SEM images of wear tracks taken from different regions and at different magnifications of same track. (c) Effect of normal load on coefficient of friction at room temperature (25 °C). (d) Effect of temperature on coefficient of friction at a constant normal load of 4 N. Samples made from Danish beech wood.

at room temperature. This value is higher than the reported values for similar materials (in range of 10^{-6})[30] and is comparable to results reported by Sang et al.[29] In the literature, the lower wear rates have been explained by the formation of carbon debris during sliding and presence of carbon in the EDX spectrum collected from the wear track. However, we have found a negligible amount of carbon in Raman spectra collected from the wear track.

4. Conclusions

All the samples made in the present work with silicon impregnation of a porous charcoal skeleton coming from natural wooden samples have a composite SiC/Si character and very low specific surface areas. This is a result of the character of the reaction process. Thus the formation of SiC/Si ceramics from porous charcoal structures obtained from natural wood takes place in two stages. The first stage involves the reaction of silicon with carbon to produce crystalline SiC and the second stage continues with infiltration of the structures by molten Si until saturation. The second stage is responsible for binding the individual SiC crystallites in a matrix of silicon to constitute a single and dense unit.

The SiC in the ceramic is in the β-SiC form as confirmed by XRD and Raman studies. The density of the resulting material varies in the range of 2.0–2.3 gm/cm^{-3}. This is roughly around 3.5 times denser than the samples made with the shape memory synthesis method,[20] from similar wooden preforms, which preserves the open skeletons without filling the pores. The present samples are found to be very dense and hard with hardness values in the range 26.5–31.4 GPa.

The wear results indicated a wear rate higher than earlier reported for SiC elements, which is believed to be mostly due to the adhesive friction of amorphous Si. Coefficient of friction measurements on these composites indicated a relatively stable value over time with respect to changing temperatures and loads. Overall, it can be said that these samples, which can be made in desired shapes, are quite stable with respect to load and temperature variations, thus qualifying them for wear and abrasive applications, for cutting tool applications, and for new generation brake materials for automobiles and aircrafts. They can also be used as refractory materials. Artificially shaped elements of the hard, compact, and light weight β-SiC/Si composite material have been fabricated as shown in Fig. 9, which might be of interest for the production of more complex shapes of SiC than possible through sintering and injection molding.

Acknowledgements

The Danish Ministry for Research and Innovation, through its program for Sustainable Energy and The Environment, has funded this work with a grant to R. Dhiman, 2104-05-0073. The authors are grateful for advice and technical support from E. Skou, S. Tougaard, T. Warner, P. B. Hansen, D. Kyrping, and T. Sørensen at SDU; to N. Dam Madsen, and P. Hald, from The University of Aarhus, S. Vikram Singh from The RISØ National Laboratory, Roskilde, Denmark and to R. Bala from HPU Shimla, India.

Appendix A. Supplementary data

Supplementary data associated with this article can be found, in the online version, at doi:10.1016/j.jeurceramsoc.2011.11.029.

References

1. Li Z, Zhang Z, Meng A, Guo J. Large-area highly-oriented SiC nanowire arrays: synthesis, Raman, and photoluminescence properties. *J Phys Chem B* 2006;**110**:22382–6.
2. Ju Z, Ma X, Fan N, Li P, Xu L, Qian Y. High-yield synthesis of single-crystalline 3C–SiC nanowires by a facile autoclave route. *Mater Lett* 2007;**61**:3913–5.
3. Fissel A, Schroter B, Richter W. Low-temperature growth of SiC thin films on Si and 6H–SiC by solid-source molecular beam epitaxy. *Appl Phys Lett* 1995;**66**:3182–4.
4. Choyke WJ, Pensk G. Physical properties of SiC. *Mater Res Soc Bull* 1997;**22**:25–9.
5. Srinivasan AV, Haritos GK, Biomimetics Hedberg FL. Advancing man-made materials through guidance from nature. *Appl Mech Rev* 1991;**44**:463–81.
6. Shin Y, Wang C, Exarhos GJ. Synthesis of SiC ceramics by the carbothermal reduction of mineralized wood with silica. *Adv Mater* 2005;**17**:73–7.
7. Calvert P. Biomimetic ceramics and composites. *Mater Res Soc Bull* 1992;**17**:37–40.
8. Dhiman R, Johnson E, Morgen P. Growth of SiC nanowhiskers from wooden precursors, separation, and characterization. *Ceram Int* 2010, doi:10.1016/j.ceramint.2011.06.001.
9. Nayak BB, Mohanty BC, Singh SK. Synthesis of silicon carbide from rice husk in a dc arc plasma reactor. *J Am Ceram Soc* 1996;**79**:1197–200.
10. Amirthan G, Udayakumar A, Prasad VVB, Balasubramanian M. Synthesis and characterization of Si/SiC ceramics prepared using cotton fabric. *Ceram Int* 2009;**35**:967–73.
11. Shin DW, Park SS, Choa YH, Niihara K. Si/SiC composites fabricated by infiltration of a Si melt into charcoal. *J Am Ceram Soc* 1999;**82**:3251–3.
12. Singh M. Environmental conscious ceramics (Ecoceramics). *Ceram Eng Sci Proc* 2000;**21**:39–44.
13. Greil P, Thomas L, Kaindl A. Biomorphic cellular silicon carbide ceramics from wood. I. Processing and microstructure. *J Eur Ceram Soc* 1998;**18**:1961–73.
14. Greil P, Thomas L, Kaindl A. Biomorphic cellular silicon carbide ceramics from wood. II. Mechanical properties. *J Eur Ceram Soc* 1998;**18**:1975–83.
15. Ota T, Takahashi M, Hibi T, Ozawa M, Suzuki S, Hikichi Y. Biomimetic process for producing SiC from wood. *J Am Ceram Soc* 1995;**78**:3409–11.
16. Chakrabarti OP, Maiti HS, Majumdar R. Si–SiC ceramics from plant precursor. *J Mater Sci* 2004;**39**:4715–7.
17. Vogli E, Sieber H, Greil P. Biomorphic SiC-ceramic prepared by Si-vapor phaseinfiltration of wood. *J Eur Ceram Soc* 2002;**22**:2663–8.
18. Locs J, Berzina-Cimdina L, Zhurish A, Loca D. Optimized vacuum/pressure sol impregnation processing of wood for the synthesis of porous, biomorphic SiC ceramics. *J Eur Ceram Soc* 2009;**29**:1513–9.
19. Vogli E, Mukerji J, Hoffman C, Kladny R, Sieber H, Greil P. Conversion of oak to cellular silicon carbide ceramic by gas-phase reaction with silicon monoxide. *J Am Ceram Soc* 2001;**84**:1236–40.
20. Dhiman R, Petrunin V, Rana K, Morgen P. Conversion of wooden structures into porous SiC with shape memory synthesis. *Ceram Int* 2010, doi:10.1016/j.ceramint.2011.05.124.
21. Zollfrank C, Sieber H. Microstructure evolution and reaction mechanism of biomorphous SiSiC ceramics. *J Am Ceram Soc* 2005;**88**:51–8.
22. Stadler Z, Krnel K, Kosmac T. Friction behavior of sintered metallic brake pads on a C/C–SiC composite brake disc. *J Eur Ceram Soc* 2007;**27**:1411–7.
23. López OB, Ortiz AL, Guiberteau F, Padture NP. Microstructural design of sliding-wear-resistant liquid-phase-sintered SiC: an overview. *J Eur Ceram Soc* 2007;**27**:3351–7.
24. Zum Gahr KH, Blattner R, Hwang DH, Pöhlmann K. Micro- and macro-tribological properties of SiC ceramics in sliding contact. *Wear* 2001;**250**:299–310.
25. Wasche R, Klaffke D, Troczynski T. Tribological performance of SiC and TiB_2 against SiC and Al_2O_3 at low sliding speeds. *Wear* 2004;**256**:695–704.
26. Dong X, Jahanmir S, Ives LK. Wear transition diagram for silicon carbide. *Tribol Int* 1995;**28**:559–72.
27. Takadoum J, Zsiga Z, Rhouma MB, Carmes CR. Correlation between friction coefficient and wear mechanism of SiC/SiC system. *J Mater Sci Lett* 1994;**13**:474–6.
28. Fouquet S, Rollin M, Pailler R, Bourrat X. Tribological behavior of composites made of carbon fibres and ceramic matrix in Si–C system. *Wear* 2008;**264**:850–6.
29. Sang K, Jin Z. Unlubricated wear of Si/SiC and its composite with nickel Si/SiC–Ni. *Tribol Int* 2001;**34**:315–9.
30. Amirthan G, Balasubramanian M. Reciprocating sliding wear studies on Si/SiC ceramic composites. *Wear* 2011, doi:10.1016/j.wear.2011.04.006.
31. Novak S, Rade K, Konig K, Boccaccini AR. Electrophoretic deposition in the production of SiC/SiC composites for fusion reactor applications. *J Eur Ceram Soc* 2008;**28**:2801–7.
32. Muroga T, Gasparotto M, Zinkle SJ. Overview of materials research for fusion reactors. *Fusion Eng Des* 2002;**61–62**:13–25.
33. Tavassoli AAF. Present limits and improvements of structural materials for fusion reactors—a review. *J Nucl Mater* 2002;**302**:73–8.
34. Byrne CE, Nagle DC. Carbonization of wood for advanced materials applications. *Carbon* 1997;**35**:259–66.
35. Paris O, Zollfrank C, Zickler GA. Decomposition and carbonisation of wood biopolymers—a microstructural study of softwood pyrolysis. *Carbon* 2005;**43**:53–66.
36. Shafizadeh F, Sekiguchi Y. Development of aromaticity in cellulosic chars. *Carbon* 1983;**21**:511–6.
37. Williamson GK, Hall WH. X-ray line broadening from filed aluminium and wolfram. *Acta Metall* 1953;**1**:22–31.
38. Shaffer PTB. A review of the structure of silicon carbide. *Acta Crystallogr B* 1969;**25**:477–88.
39. Fromm J. Wood formation of trees in relation to potassium and calcium nutrition. *Tree Physiol* 2010;**30**:1140–7.
40. Tougaard S. Energy loss in XPS: fundamental processes and applications for quantification, non-destructive depth profiling and 3D imaging. J Electr Spectrosc Relat Phenom 178–179: 128–53.
41. Ziegler JF. SRIM-2003. *Nucl Instr Meth B* 2004;**219–220**:1027–36.
42. Ziegler JF. SRIM—the stopping and range of ions in matter. <http://www.srim.org>; 2009.
43. Nakashima S, Higashihira M, Maeda K. Raman scattering characterization of polytype in silicon carbide ceramics: comparison with X-ray diffraction. *J Am Ceram Soc* 2003;**86**:823–9.
44. Bechelany M, Brioude A, Cornu D, Ferro G, Miele P. A Raman spectroscopy study of individual SiC nanowires. *Adv Funct Mater* 2007;**17**:939–43.
45. Oliver WC, Pharr GM. An improved technique for determining hardness and elastic-modulus using load and displacement sensing indentation experiments. *J Mater Res* 1992;**7**:1564–83.
46. Bolshakov A, Pharr GM. Influences of pile-up on the measurement of mechanical properties by load and depth sensing indentation techniques. *J Mater Res* 1998;**13**:1049–58.
47. Pharr GM. Measurement of mechanical properties by ultra-low load indentation. *Mater Sci Eng A* 1998;**253**:15–9.
48. Sanghoon S, Jang J, Pharr GM. Extraction of flow properties of single-crystal silicon carbide by nanoindentation and finite-element simulation. *Acta Mater* 2008;**56**:3824–32.
49. Vandeperre LJ, Giuliani F, Lloyd SJ, Clegg WJ. The hardness of silicon and germanium. *Acta Mater* 2007;**55**:6307–15.